

X-Ray and Neutron Diffraction Measurements of Dislocation Density and Subgrain Size in a Friction-Stir-Welded Aluminum Alloy

WANCHUCK WOO, TAMÁS UNGÁR, ZHILI FENG, EDWARD KENIK,
and BJØRN CLAUSEN

The dislocation density and subgrain size were determined in the base material and friction-stir welds of 6061-T6 aluminum alloy. High-resolution X-ray diffraction measurement was performed in the base material. The result of the line profile analysis of the X-ray diffraction peak shows that the dislocation density is about $4.5 \times 10^{14} \text{ m}^{-2}$ and the subgrain size is about 200 nm. Meanwhile, neutron diffraction measurements have been performed to observe the diffraction peaks during friction-stir welding (FSW). The deep penetration capability of the neutron enables us to measure the peaks from the midplane of the Al plate underneath the tool shoulder of the friction-stir welds. The peak broadening analysis result using the Williamson–Hall method shows the dislocation density of about $3.2 \times 10^{15} \text{ m}^{-2}$ and subgrain size of about 160 nm. The significant increase of the dislocation density is likely due to the severe plastic deformation during FSW. This study provides an insight into understanding the transient behavior of the microstructure under severe thermomechanical deformation.

DOI: 10.1007/s11661-009-9963-5

© The Minerals, Metals & Materials Society and ASM International 2009

I. INTRODUCTION

IN many thermomechanical engineering processes, the severe plastic deformation results in a large amount of dislocations in microstructure.^[1,2] It has been reported that the dislocation-embedded “grain structure” is subjected to lattice distortions and strains within grains of materials.^[3,4] This is the case for friction-stir welding (FSW). Friction-stir welding is a solid-state joining method using a rotating tool consisting of a threaded pin and tool shoulder to apply the severe plastic deformation and frictional heating into the joining materials.^[5] During FSW, the materials softened by heat underneath the rotating tool shoulder flow around the tool pin column with pressure and

consolidate behind the tool to form a solid-state continuous region.^[6] As a result, friction-stir welds show a unique grain structure influenced by severe thermomechanical deformation, recovery, or recrystallization at elevated temperatures during welding.^[7–11]

The microstructure of friction-stir welds is one of the most important welding research areas. Although the microstructure of FSW has been extensively studied, very limited quantitative analysis of the grain structure in terms of the dislocation density and subgrain size is available to date. Detailed information of the grain structure is necessary in the friction-stir welds, because the grain structure (dislocation density and subgrain size) can significantly affect the plastic deformation behaviors after yielding such as strain-hardening rate and hardening capacity in welds.^[12] The grain morphologies and dislocation structures have been observed on various friction-stir weld alloys mainly using transmission electron microscopy (TEM), but typical observations rely on the “postmortem” analysis method, which examines the material after processing. Recently, the transient materials behavior “during” processing has been focused in order to understand the evolution and the final microstructure characteristics.

In-situ observation of microstructure changes has been extremely challenging, and many measurement techniques are not applicable. In order to observe the transient microstructure changes during FSW, the deep penetration capability of the neutron diffraction is necessary. In the current study, for example, the neutron beam needs to penetrate through about 12-mm thickness of the FSW machine tool and diffract from the FSW Al alloy underneath the machine tool. One major issue in neutron diffraction is the relatively weak

WANCHUCK WOO, formerly Postdoctoral Research Associate, with the Materials Science and Technology Division, Oak Ridge National Laboratory, Oak Ridge, TN 37831, is Senior Researcher, with the Neutron Science Division, Korea Atomic Energy Research Institute, Daejeon, 305-353, South Korea. Contact e-mail: chuck-woo@kaeri.re.kr TAMÁS UNGÁR, Professor, is with the Department of General Physics, Eötvös University, H-1518, Budapest, Hungary. ZHILI FENG, Group Leader, and EDWARD KENIK, Senior Researcher, are with the Materials Science and Technology Division, Oak Ridge National Laboratory, Oak Ridge, TN 37831. BJØRN CLAUSEN, Instrument Scientist, is with Los Alamos Neutron Science Center, Los Alamos National Laboratory, Los Alamos, NM 87545.

This article is based on a presentation given in the symposium “Neutron and X-Ray Studies of Advanced Materials,” which occurred February 15–19, 2009, during the TMS Annual Meeting in San Francisco, CA, under the auspices of TMS, TMS Structural Materials Division, TMS/ASM Mechanical Behavior of Materials Committee, TMS: Advanced Characterization, Testing, and Simulation Committee, and TMS: Titanium Committee.

neutron fluxes causing difficulties in *in-situ* observation of the fast, dynamic material behavior. Thus, *in-situ* neutron diffraction study of transient materials behavior requires a completely different experimental approach from the conventional study of static problems such as residual stress measurements. For this purpose, we recently developed an *in-situ* time-resolved neutron diffraction method, which drastically improves the temporal resolution of neutron diffraction and enables observations of the transient microstructural changes during FSW.^[13,14] In order to achieve sufficient temporal resolution, the entire Al sample plate was continuously traversed, creating the quasi-steady state of material during FSW.^[15] To this end, the required temporal resolution of the typical neutron-diffraction measurements (over 20 minutes) can be achieved and, thereby, overcome the limitation of the temporal resolution in neutron-diffraction measurements.

Line broadening analysis of the diffraction peak profile is a well-established technique for the determination of microstructure in terms of dislocation density and subgrain size in crystalline materials.^[16–22] The Williamson–Hall peak analysis method suggests that diffraction peak profiles broaden when subgrains (or crystallites) are small or if the crystal lattice is distorted by lattice defects, especially by dislocations.^[16,17] The size and strain influences on diffraction peak broadening can be evaluated separately on the basis of their different *hkl* dependences.^[18,19] For example, the convolutional multiple whole profile (CMWP) fitting procedure has been used to evaluate diffraction peak patterns.^[20] In the CMWP, a theoretical peak pattern can be simulated based on the two defect-related profile functions. It convolutes the size and strain effect on the diffraction peak profiles for a dislocated crystal.^[21] Consequently, the simulated and measured diffraction patterns are compared to each other by a nonlinear least-squares method and provide the microstructural characteristics. Details are described elsewhere.^[18–22]

In this study, we determined the dislocation density and subgrain size in (1) the base material (6061-T6 Al alloy) using the high-resolution X-ray diffraction and neutron diffraction, and (2) the severely deforming zone (stir zone) during FSW using *in-situ* time-resolved neutron diffraction. The diffraction peaks measured by X-ray and neutron diffractions were analyzed using the CMWP and Williamson–Hall peak broadening analysis methods, respectively.

II. EXPERIMENTAL DETAILS

A. Material

As-received commercial 6061-T6 Al alloy rolled plate was solution heat treated and aged for 6 hours at 185 °C. The nominal chemical composition in weight percent is 1.0Mg, 0.6Si, 0.3Cu, and balance Al. Grains of about 200- μ m size were elongated along the rolling direction with a typical recrystallized rolling texture. The cross section of the base material and severely thermomechanically deformed region (stir zone) of

friction-stir welds was cold mounted, polished, and etched with Keller's reagent for optical microscopy at room temperature. The grain structure including dislocations was observed from the base material and friction-stir welds using TEM. The disc-type specimens (3 mm in diameter) were prepared by electrical discharge machining (EDM), mechanical grinding to 100- μ m thickness, and electropolishing using a 30 pct nitric acid solution in methanol with 25 voltages for 20 seconds at –30 °C.

B. X-Ray Diffraction Measurements

The grain structure of the base material (Al 6061-T6) was measured using X-ray diffraction line profile analysis. The high-resolution microbeam X-ray diffractometer^[21] (Nonius FR591) was used with a rotating copper anode (Cu $K_{\alpha 1}$) radiation (wavelength, $\lambda = 0.15406$ nm). The X-ray beam size is about 0.1×1 mm on the sample, and the scattered radiation is registered by four different position-sensitive imaging detectors located at 300 to 600 mm from the base material. The scattered radiation covered about $2\theta = 30$ to 150 deg of the angular range of diffractions.

C. FSW and In-Situ Neutron-Diffraction Measurements

We specially designed an FSW machine in real engineering scale. The machine was remotely operated and mounted on the translation stage of the Spectrometer for Materials Research at Temperature and Stress (SMARTS) at Los Alamos Neutron Science Center.^[23] The FSW was made on 6.35-mm-thick 6061-T6 Al alloy plate. The plate sample was continuously traversed at a constant traveling speed of 0.42 mm/s as the tool was rotated at 156 rev/min with a pressure into the sample surface to impose the severe thermomechanical deformation on materials. The transverse sides of the plate sample were clamped to constrain the displacement during processing, and the clamping was removed after air cooling to 25 °C. In the end, a 760-mm long and 25-mm wide deformation region was made along the middle of the plate width. The hard tool made of an H-13 steel and the diameter of the threaded pin and the tool shoulder were 6.35 and 25.4 mm, respectively. The specimen of the Al plate was 965-mm long (*x*), 178-mm wide (*y*), and 6.35-mm thick (*z*).

We measured diffraction peaks based on the quasi-steady state of material described in Reference 15. The quasi-steady state is an energy equilibrium state, which does not change the material's behavior as a function of time. In order to create the quasi-steady state, the entire Al sample plate was continuously traversed along the *x* direction, and simultaneously, the neutron diffraction measurements were performed as the deformation zone was being made (Figure 1). The incident neutron beam was focused on a predetermined measurement location (8 mm behind the tool center). The detector collected the diffraction peaks from the defined scattering volume with a scattering vector parallel to the normal direction of the plate using a scattering volume of 12 mm³ defined by the 2 (*x*) \times 2 (*y*) mm² square slit of the incident beam

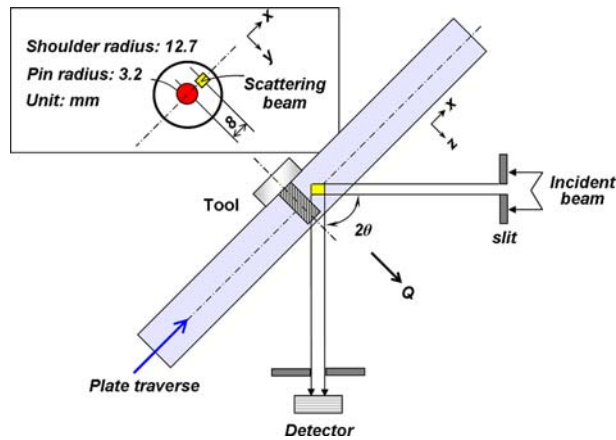


Fig. 1—Experimental setup of the *in-situ* time-resolved neutron diffraction measurement during FSW. The FSW machine was mounted on the neutron diffractometer, and real-time measurements were performed as the rotating FSW tool imposed severe thermomechanical deformation on the sample. The inset presents the location of the neutron beam, which was predetermined at 8 mm behind the tool center underneath the tool shoulder.

and the 3 (z) mm wide radial collimator. The long plate sample dimension (965-mm long) allowed achievement of over 20 minutes of quasi-steady state during FSW. In addition, a neutron diffraction measurement was performed in the base material. The purpose is to obtain the initial state (background) of the neutron diffraction peak profiles from the base material. Consequently, the peak broadening of the neutron diffraction measurement was compared to that of the X-ray results measured using base material.

III. RESULTS AND DISCUSSION

A. Microstructure Analysis

Figure 2 shows the microstructure of the cross section of the base material (a commercial 6061-T6 aluminum alloy rolled plate) and FSW 6061-T6 Al alloy. The average grain sizes were measured at the base material and FSW (stir zone) using optical microscopy showing about 120 μm and 5 μm grain size, respectively, using the linear intercept method (Figures 2(a) and 2(b)).

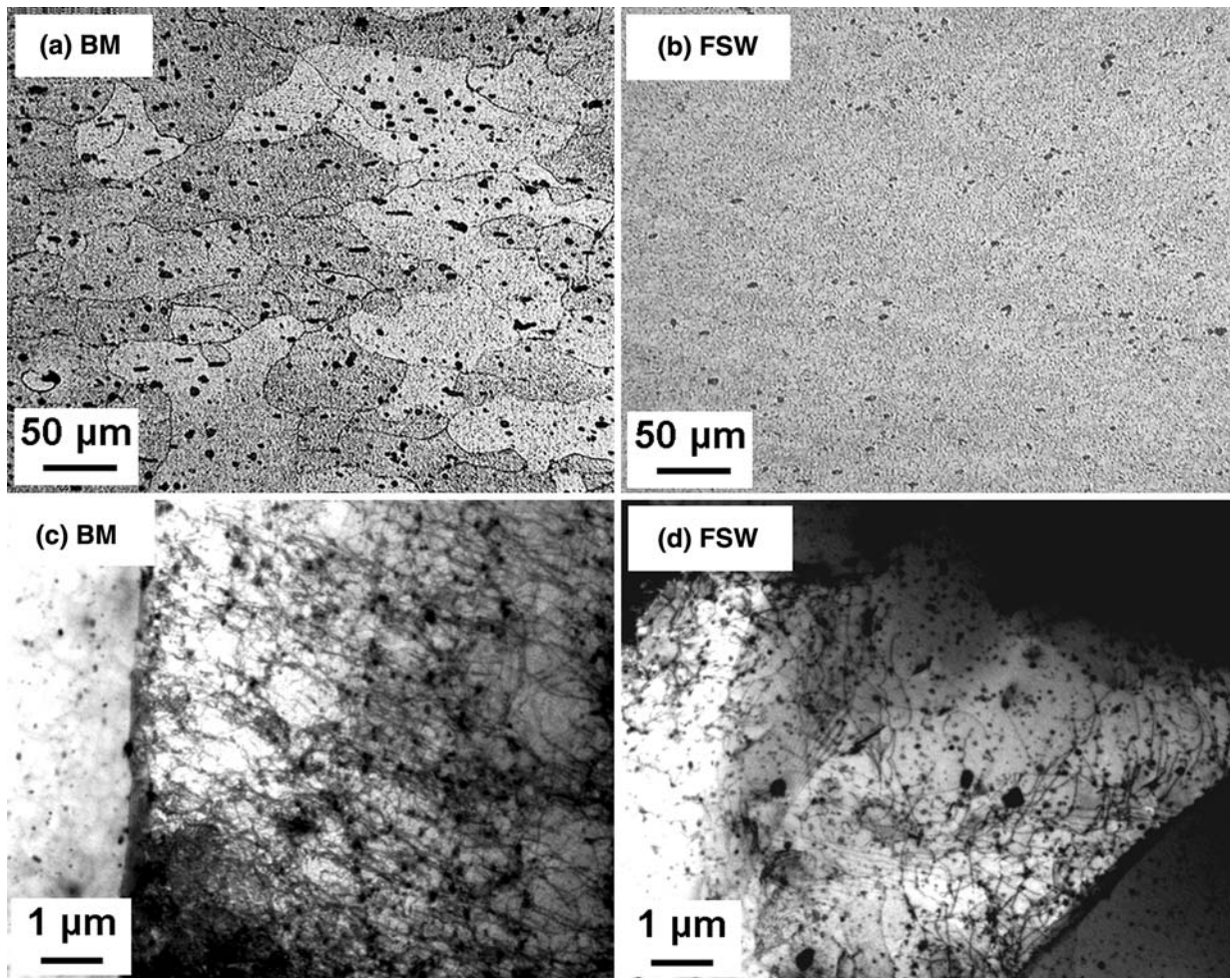


Fig. 2—Microscopy of the 6061-T6 Al alloy: (a) base material and (b) FSW (stir zone). The TEM bright-field images of (c) base material and (d) FSW. The black line segments and dots indicate dislocations and precipitates in the TEM grain structure, respectively.

Two TEM bright-field images are also shown in Figure 2. The images show the dislocation structure embedded grains of the base material (Figure 2(c)) and the thermomechanically deformed stir zone of FSW (Figure 2(d)). The comparison shows that the as-received rolled Al plate sample contains a larger number of dislocations (black line segments) and the FSW (stir zone) has less dislocation. The low dislocation density in FSW is likely due to the dynamic recrystallization during FSW.^[8,9]

B. X-Ray Diffraction Peak Profile Analysis

Figure 3(a) shows the X-ray diffractogram measured at the base material (6061-T6 Al alloy). The X-ray diffraction peak profiles were evaluated by the CMWP full pattern fitting procedure. The open circles are the directly measured diffraction peak data and the solid line is a fitted curve using the theoretical diffraction functions obtained by the CMWP fitting procedure.^[20,21] The

indices of each (hkl) reflection are presented for the fcc Al alloy, and the difference between the measured and fitted patterns is shown in the lower part of the figure, which shows a good fitting result between the measured and theoretically simulated profiles. Using the comparison between the measured profiles and theoretically calculated diffraction profiles, the CMWP procedure numerically provides the following independent parameters for the microstructure characterization in the current base material:^[20] (1) the median (m , 110 ± 10 nm) and (2) the variance (σ , 0.51 ± 0.05) of the log-normal size distribution function, (3) the mean subgrain size $\langle x \rangle_{\text{area}}$, and (4) the dislocation density (ρ). Note that the area-weighted mean subgrain size can be calculated using the following equation with the assumption of spherical crystallites and a log-normal crystallite size distribution:^[21]

$$\langle x \rangle_{\text{area}} = m \exp(2.5\sigma^2) \quad [1]$$

Note that the crystallite size obtained using diffraction can be equivalent (or similar) to the mean size of domains such as subgrains or dislocation cells due to the coherently scattered X-rays or neutrons from such domains in severely deformed materials.^[18–21] Using the CMWP procedure, the numerically calculated dislocation densities and average subgrain size are about $4.5 \pm 0.5 \times 10^{14} \text{ m}^{-2}$ and 200 ± 20 nm, respectively, in the base material.

The Williamson–Hall plot shows the qualitative behavior of diffraction peak broadening using the full-width at half-maximum (FWHM) as a function of K , where $K = 2 \sin \theta / \lambda$, and θ and λ are the diffraction angle and the wavelength of the X-ray, respectively.^[18] The FWHMs are plotted as $\Delta K = 2 \cos \theta (\Delta \theta) / \lambda$ in $1/\text{nm}$ scale, where $\Delta \theta$ is the FWHM obtained from each (hkl) peak in Figure 3(a). Note that the C is the dislocation contrast factor, which is determined by the elastic anisotropy and the dislocation type of the material (details in Section III). Consequently, Figure 3(b) shows the *modified* Williamson–Hall plot of the base material presenting the line broadening (ΔK) behavior among the different (hkl) peaks.

C. Neutron Diffraction Peak Profile Analysis

In order to study the transient material's behavior, the neutron diffraction measurements were performed underneath the tool shoulder during FSW. Figure 4(a) show the neutron diffraction peaks measured in the base material and during FSW. The measured diffraction peaks in the raw data were analyzed using the single peak fitting method, which refines each (hkl) reflection of the measured diffraction peaks in the general structure analysis system (GSAS).^[24] It determines the interplanar spacing (d spacing), peak intensity, and peak broadening among the different (hkl) grains.

The Williamson–Hall peak broadening analysis suggests that broadening of the diffraction peak profile (ΔK , nm^{-1}) can be written as a combination of the grain size ($0.9/D$) and strain (ΔK^D) effects:^[17] $\Delta K = 0.9/D + \Delta K^D$, where $K = 1/d$, $\Delta K = -K(\Delta d/d)$, and D is the

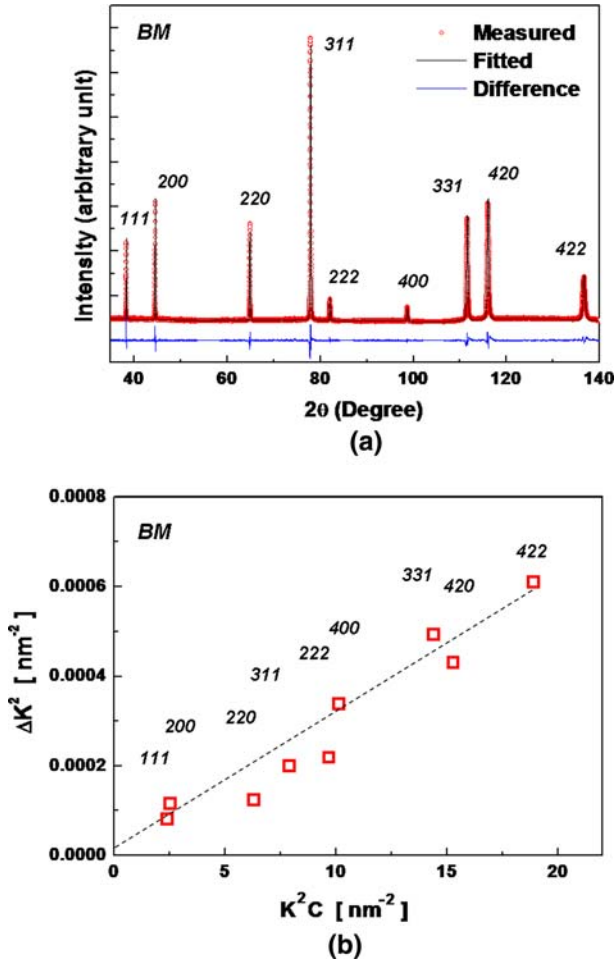


Fig. 3—(a) X-ray diffraction measured (open circles) and CMWP procedure fitted (solid line) patterns among each (hkl) in the base material of Al 6061-T6 alloy. (b) Peak broadening analysis using the *modified* Williamson–Hall plot. The FWHM (ΔK) in each (hkl) peak is presented as a function of $KC^{1/2}$ (K is defined as $2 \sin \theta / \lambda$, where θ and λ are the X-ray diffraction angle and the wavelength, respectively, and C is the dislocation contrast factor).

average subgrain (crystallite) size. The d (nm) is the d spacing and Δd (nm) is the FWHM obtained from the single peak fitting of the diffraction data. The Williamson–Hall plot has been modified replacing K by K^2C based on the following equation:^[18–20]

$$(\Delta K)^2 = (0.9/D)^2 + (\pi A^2 b^2 / 2) \rho (K^2 C) + O(K^2 C)^2 \quad [2]$$

where A is a constant depending on the effective outer cutoff radius of dislocations, b is the Burgers vector of dislocation (0.286 nm in Al), ρ is the dislocation density, and O indicates noninterpreted higher-order terms. Strain anisotropy among each (hkl) reflection has been rationalized by the dislocation contrast factor (C) in the modified Williamson–Hall plot (Figure 4(b)).

The dislocation contrast factor (C_{hkl}) becomes a linear function of the (hkl) invariant of the reflections. In the polycrystalline fcc Al metal, $C_{hkl} = 0.2[1 - q(h^2k^2 + h^2l^2 + k^2l^2)/(h^2 + k^2 + l^2)^2]$, where 0.2 is the average

dislocation contrast factor determined by the elastic anisotropy factor, dislocation type, and single-crystal elastic constants (obtained from Figure 1 in Reference 19). Hence, C_{hkl} is presented as a function of the q parameter in each (hkl) reflection. Putting C_{hkl} into Eq. [2] yields the theoretical calculation of ΔK . The theoretically calculated ΔK and each constant coefficient including parameter q can be determined when the difference between the calculated and measured ΔK values is the minimum using the least-squares fitting method.^[21] As a result, ΔK was modified and fitted among the (hkl) reflections as a function of K^2C , as shown in Figure 4(b).

It is worth noting that stress fields varying over grains (known as intergranular or type II stresses) can also cause peak broadening.^[25] However, the microstress-related peak broadening may not be significant due to the isotropic thermal, elastic/plastic properties and resultant low interactions among grains in the case of Al alloys.^[26]

D. Dislocation Density and Subgrain Size

The modified Williamson–Hall plot (Figure 4(b)) provides two important microstructural features.^[18,19] First, the slope of the linear regression is proportional to the microstrain. The slope corresponding to the FSW is considerably higher than that of the base material, which indicates much larger microstrains mainly caused by dislocations during FSW. Second, the intercept of the linear regression through the data points at $K = 0$ is a rough size estimation of the coherent scattering domains such as the subgrain size of the microstructure. Accordingly, the fitting curves provide the intercept constant, $(0.9/D)^2$, and the slope of the fitting curve, $(\pi A^2 b^2 / 2) \rho$, in the base material and friction-stir weld. The results were summarized in Table I.

In order to calculate the dislocation density, it is necessary to determine the A value of the second coefficient $(\pi A^2 b^2 \rho / 2)$ in Eq. [2]. Presumably the dislocation density of the base material is identical when measured using both the neutron and X-ray diffraction methods. Thus, the dislocation density ($\rho = 4.5 \pm 0.5 \times 10^{14} \text{ m}^{-2}$) in the X-ray diffraction is equal to the

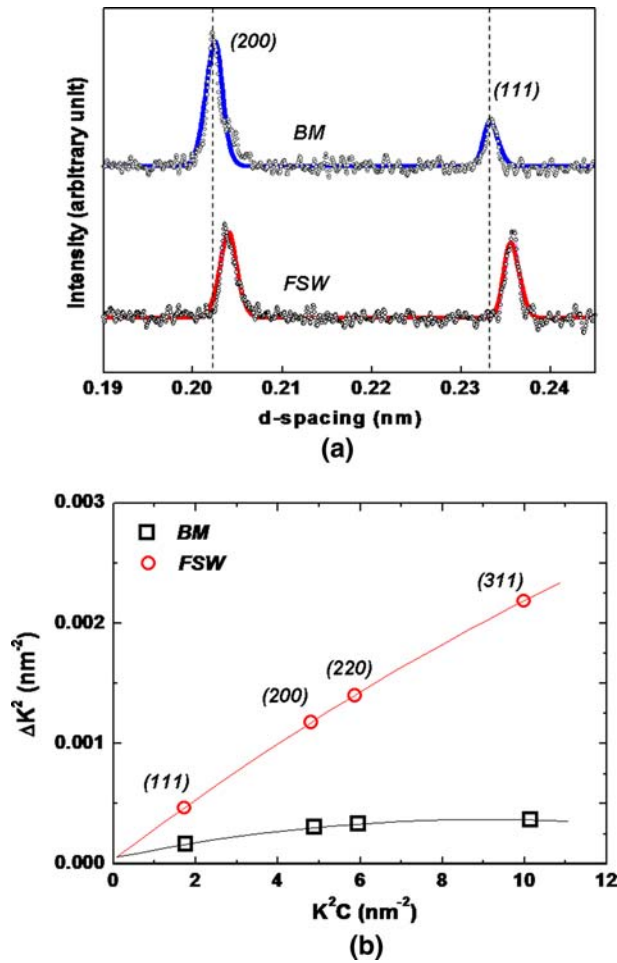


Fig. 4—(a) Neutron diffraction patterns in the (111) and (200) reflections. The gray dots indicate the directly measured neutron diffraction results, and the overlapped profiles are Rietveld peak refinements using GSAS. The neutron diffraction patterns were measured from the base material (BM) and during FSW. (b) Peak broadening analysis using the modified Williamson–Hall plot. The K is defined as $1/d$ (d is the d spacing in each hkl peak), ΔK is driven as $-K(\Delta d/d)$ (Δd is the FWHM obtained in the neutron diffraction peak), and C is the dislocation contrast factor.

Table I. Summary of the Coefficient of the Fitting Curve in the Modified Williamson–Hall Plot (Figure 4(b)) in the Base Material and FSW*

	Base Material	During FSW	After FSW (Ref. 22)
$(0.9/d)^2$	2.0×10^{-5}	3.6×10^{-5}	—
$(\pi A^2 b^2 / 2) \rho$	3.6×10^{-5}	2.6×10^{-4}	—
Subgrain size (nm)	200	160	180
Dislocation density (m^{-2})	4.5×10^{14}	3.2×10^{15}	1.0×10^{14}

*The intercept of the linear regression and the slope of the linear regression in the fitting curve are equivalent to the $(0.9/D)^2$ and $(\pi A^2 b^2 / 2) \rho$ terms in Eq. [2], respectively. Each term determines the subgrain size and dislocation density in the base material and during FSW of the Al 6061-T6 alloy. For comparison, the dislocation density after FSW is included (Ref. 22).

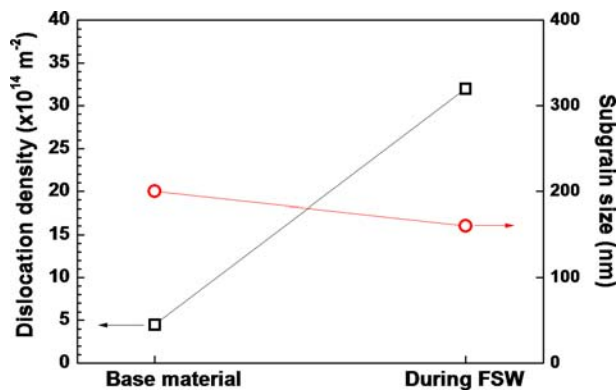


Fig. 5—Dislocation density and subgrain size in the base material and during FSW of the Al 6061-T6 alloy. The interception of the fitted curve (Fig. 4(b)) provides a subgrain size (when $K = 0$ in Eq. [2]), and the slope of the fitting curve determines the dislocation density.

second coefficient ($\pi A^2 b^2 \rho / 2$) from the fitting result, which determines the unknown constant A as 0.63. Note that this value was applied for the calculation of the dislocation density during FSW.

As a result, Figure 5 shows the dislocation density and subgrain size in the base material and FSW 6061-T6 Al alloy using neutron diffraction. The analysis results were also summarized in Table I. Compared to the initial dislocation density ($4.5 \times 10^{14} \text{ m}^{-2}$), which could be found in the typical as-received rolled Al plate,^[27] a significant increase of the dislocation density is obvious up to $3.2 \times 10^{15} \text{ m}^{-2}$ during FSW. It is likely that the measurement location (underneath the tool shoulder at 8 mm from the tool centerline) experiences severe straining and deformation with high strain rates. It is also significantly high when compared to the previous result of dislocation density, which was measured after FSW ($1 \times 10^{14} \text{ m}^{-2}$).^[22] Meanwhile, there is no significant change in the subgrain size (160 nm) during FSW compared to the base material (200 nm). It has been reported that the crystallite (particle) size obtained using diffraction methods can be equivalent to the mean size of domains such as subgrains or dislocation cells due to the coherently scattered X-rays or neutrons from such domains.^[4] Consistently, it is clear that the subgrain size (nanometer scale) measured by the neutron diffraction (Table I) is much smaller than the grain size (micrometer scale) observed in Figure 2.

The dislocation density of the grain structure can significantly influence the strain-hardening behavior associated with dislocation movements during tensile deformation in FSW.^[22] Therefore, this *in-situ* observation of transient microstructure is important in understanding the complicated FSW process, which includes the severe plastic deformation and dynamic recrystallization at elevated temperature.

IV. CONCLUSIONS

The dislocation density and subgrain size were determined in the base material and FSW 6061-T6 Al alloy.

In-situ time-resolved neutron diffraction measurements were performed during FSW. The diffraction peak broadening analysis using the modified Williamson–Hall plot quantifies the dislocation density during FSW of about $3.2 \times 10^{15} \text{ m}^{-2}$ and the average subgrain size of about 160 nm. The dislocation density during FSW is 7 times higher than the initial dislocation density ($4.5 \times 10^{14} \text{ m}^{-2}$) of the base material. The significant increase of the dislocation density during FSW is most likely due to the severe plastic deformation imposed by the stirring tool pin. This study shows the fast, transient grain structure inside a bulk Al alloy during FSW with the help of the *in-situ* time-resolved neutron diffraction measurement method.

ACKNOWLEDGMENTS

This research is sponsored by the Laboratory Directed Research and Development programme of Oak Ridge National Laboratory, managed by UT–Battelle, LLC for the United States Department of Energy under Contract No. DE-AC05-00OR22725. Research at the Oak Ridge National Laboratory SHaRE User Center was supported by the Division of Materials Sciences and Engineering, Office of Basic Energy Sciences, United States Department of Energy, under Contract No. DE-AC05-00OR22725 with UT–Battelle, LLC. One of the authors (WW) is supported by the Nuclear Research and Development Program, Korea Science and Engineering Foundation, funded by the Korean government. TU is grateful to the Hungarian National Science Foundation OTKA Nos. 71594 and 67692. The authors also thank L. Balogh, T.A. Sisneros, and D.W. Brown for their help.

REFERENCES

1. Y. Wang, M. Chen, F. Zhou, and E. Ma: *Nature*, 2002, vol. 419, pp. 912–15.
2. R. Valiev: *Nat. Mater.*, 2004, vol. 3, pp. 511–16.
3. M.A. Krivogla: *Theory of X-ray and Thermal Neutron Scattering by Real Crystals*, Plenum Press, New York, NY, 1996.
4. B.D. Cullity and S.R. Stock: *Elements of X-ray Diffraction*, Prentice Hall, Upper Saddle River, NJ, 2001.
5. M.W. Mahoney, C.G. Rhodes, J.G. Flintoff, R.A. Spurling, and W.H. Bingle: *Mater. Trans. A*, 1998, vol. 29, pp. 1955–64.
6. R.S. Mishra and Z.Y. MA: *Mater. Sci. Eng. R*, 2005, vol. 50, pp. 1–78.
7. L.E. Murr, G. Liu, and J.C. McClure: *J. Mater. Sci.*, 1998, vol. 33, pp. 1243–51.
8. K.V. Jata and S.L. Semiatin: *Scripta Mater.*, 2000, vol. 43, pp. 743–49.
9. J.Q. Su, T.W. Nelson, R. Mishra, and M. Mahoney: *Acta Mater.*, 2003, vol. 53, pp. 713–29.
10. P.B. Prangnell and C.P. Heason: *Acta Mater.*, 2005, vol. 53, pp. 3179–92.
11. W. Woo, H. Choo, D.W. Brown, and Z. Feng: *Metall. Mater. Trans. A*, 2007, vol. 38, pp. 69–76.
12. A. Simar, Y. Bréchet, B. de Meester, A. Denquin, and T. Pardoen: *Acta Mater.*, 2007, vol. 55, pp. 6133–43.
13. W. Woo, Z. Feng, X.-L. Wang, K. An, H. Choo, C.R. Hubbard, and S.A. David: *Appl. Phys. Lett.*, 2006, vol. 88, p. 248623.
14. W. Woo, Z. Feng, X.-L. Wang, D.W. Brown, B. Clausen, K. An, H. Choo, C.R. Hubbard, and S.A. David: *Sci. Technol. Weld. Join.*, 2007, vol. 12, pp. 298–303.

15. W. Woo, Z. Feng, X.-L. Wang, K. An, W.B. Bailey, S.A. David, C.R. Hubbard, and H. Choo: *Residual Stresses VII*, 2006, vols. 524–525, pp. 387–92.
16. B.E. Warren and B.L. Averbach: *J. Appl. Phys.*, 1952, vol. 23, p. 497.
17. G.K. Williamson and W.H. Hall: *Acta Metall.*, 1953, vol. 1, pp. 22–31.
18. T. Ungár and A. Borbély: *Appl. Phys. Lett.*, 1996, vol. 69, pp. 3173–75.
19. T. Ungár, I. Dragomir, Á. Révész, and A. Borbély: *J. Appl. Cryst.*, 1999, vol. 32, pp. 992–1002.
20. G. Ribárik, T. Ungár, and J. Gubicza: *J. Appl. Cryst.*, 2001, vol. 34, pp. 669–76.
21. T. Ungár, J. Gubicza, G. Ribárik, and A. Borbély: *J. Appl. Cryst.*, 2001, vol. 34, pp. 298–310.
22. W. Woo, L. Balogh, T. Ungár, H. Choo, and Z. Feng: *Mater. Sci. Eng. A*, 2008, vol. 498, pp. 308–13.
23. M.A.M. Bourke, D.C. Dunand, and E. Ustundag: *Appl. Phys. A*, 2002, vol. 74, pp. S1707–S1709.
24. A.C. Larson and R.B. Von Dreele: Report No. LAUR 86-748, Los Alamos National Laboratory, Los Alamos, NM, 2004.
25. M.T. Hutchings, P.J. Withers, T.M. Holden, and T. Lorentzen: *Introduction to the Characterization of Residual Stress by Neutron Diffraction*, Taylor and Francis, Boca Raton, FL, 2005.
26. B. Clausen, T. Lorentzen, and T. Leffers: *Acta Mater.*, 1998, vol. 46, pp. 3087–98.
27. J. Gubicza, N.Q. Chinh, Z. Horita, and T.G. Langdon: *Mater. Sci. Eng. A*, 2004, vol. 387, pp. 55–59.